BEHAVIOR OF MARBLE UNDER COMPRESSION

By C.-T. Chang,[1] P. Monteiro,[2] K. Nemati,[3] and K. Shyu[4]

ABSTRACT: Results of experimental and theoretical studies of the micromechanical behavior of marble under compression are presented. A cylindrical marble specimen was submerged in a molten metal alloy under compression and the alloy was driven into voids and fractures by pore pressure. The alloy was solidified at a certain stage of the experiment in order to preserve the geometry of microcracks as they existed under load and to distinguish these cracks from those generated during sample polishing. With a surface tension of 400 mN/m, the alloy could penetrate into flat cracks with apertures as fine as 0.08 μm under a pore pressure of 10.3 MPa (1,500 psi). This technique also facilitated observation of the microcracks in three dimensions. A comprehensive image analysis was performed on the cracking pattern developed in the marble samples. The propagation of the cracking process was modeled using nonlinear discontinuous deformation analysis (DDA) with a finite-element meshed block system.

INTRODUCTION

The identification of cracks induced by loading and unloading are important in understanding the mechanisms for the generation, propagation, and interaction of stress-induced microcracks. Marble contains many discontinuities ranging from microcracks and pores through joints to bedding planes and faults. All of these discontinuities contribute to make marble strong in compression, weak in tension, and permeable to fluids.

It is important to understand how the formation, growth, and interaction of microcracks leads to macrofracture. Cracks induced under a compressive stress field are of the most interest because marbles are under compressive stress most of the time. The effect of cracks and imperfections on the behavior of rocks has been studied by many researchers. McClintock and Walsh (1962) used a Griffith approach to predict the influence of cracks on the strength of rock; Walsh (1965) developed micromechanical models to incorporate the effect of cracks on the elastic moduli of the rock; Nemat-Nasser (1985) used a geometric probability approach to characterize and analyze microcracks in rocks; and Hoek and Bieniawshi (1965) studied the brittle fracture propagation in rock under compression. The understanding of the microstructure and micromechanics of marble is becoming increasingly important for the prediction of durability and integrity of thin-set marble panels (Cohen and Monteiro 1991).

This paper presents direct observations of the size, orientation, and interaction of microcracks in a marble specimen as they exist under load. The proposed method involves the application of a metal in liquid phase, known as Wood's metal, that has a melting point below the boiling point of water, to preserve the microstructure of stress-induced microcracks in marble. Used in conjunction with scanning electron microscopy (SEM), this application has made possible the detailed observation of microcracks in marble as they exist under load.

Named after the astronomer who used an alloy of bismuth, lead, tin, and cadmium to create a perfect parabolic surface for astronomical observations, Wood's metal has been used in the past few years to study the microstructure of different materials. Yadev et al. (1984) used Wood's metal to study pore fluid porosimetry and to measure contact areas and voids between the surfaces of natural fractures. Zheng (1989) used Wood's metal to fill voids and microcracks in elastic rock specimens during loading, and solidified it before unloading to preserve the microstructure in specimens under load. Nemati (1994) used Wood's metal to study the generation and interaction of compressive stressed-induced microcracks in concrete. The advantage of such an alloy is that it can be injected into voids and stress-induced microcracks at the desired stress level, then solidified at any stage of the experiment to preserve, in three-dimensional form, the geometry of the microcracks induced at any given stage of the experiment.

This paper also develops a method to model the crack propagation of a marble sample under load. The model is based on Shi's (1988) discontinuous deformation analysis incorporated with finite-element mesh and nonlinear material behavior. As an example, an image of the crack pattern in the specimen obtained using Wood's metal technique is used as the initial configuration for the computational model. The computer simulation indicates that the model predicts crack evolution fairly well.

MODELING OF DISCONTINUOUS DEFORMATION

After the original development of the finite-element method (FEM), practical discontinuity problems were also taken into account in numerical analysis [see Zienkiewicz and Taylor (1991)]. Goodman et al. (1968) developed the "jointed element" and applied it extensively in rock engineering. Later, Cundall (1971, 1988) introduced the distinct-element method, which is now widely used for jointed or blocky rock. Unlike FEM, these two methods are force methods that incorporate fictitious forces to reach the convergence criteria of block overlapping and to reach equilibrium. The displacement-based method—discontinuous deformation analysis (DDA)—was developed by Shi (1988). The primary function of DDA is to solve large displacements and deformations of a discontinuous block system. For each block, rigid body translation and rotation accompanied by axial and shear deformations are used to describe the motion of the entire block system. Sliding, opening, and closing of block interfaces are also allowed. Like FEM, this method uses minimization of the total potential energy to reach equilibrium in the forward model. In the backward model, it uses a "least-square" minimization to back-calculate the global configuration of the block system from measured data.

In summary, DDA deals with discontinuous problems and FEM with continuous ones; the difference between a "block" in DDA and an "element" in FEM must be distinguished. For example, FEM uses nodes to link the elements together, and

[1]Postdoctoral Res., Civ. Engrg. Dept., Univ. of California, Berkeley, CA 94720.

[2]Prof., Civ. Engrg. Dept., Univ. of California, Berkeley, CA.

[3]Postdoctoral Res., Civ. Engrg. Dept., Univ. of California, Berkeley, CA.

[4]Adjunct Asst. Prof., Civ. Engrg. Dept., North Carolina Agric. and Tech. State Univ., Greensboro, NC 27411.

Note. Discussion open until January 1, 1997. To extend the closing date one month, a written request must be filed with the ASCE Manager of Journals. The manuscript for this paper was submitted for review and possible publication on June 9, 1995. This paper is part of the ***Journal of Materials in Civil Engineering***, Vol. 8, No. 3, August, 1996. ©ASCE, ISSN 0899-1561/96/0003-0157–0170/$4.00 + $.50 per page. Paper No. 10889.

common nodes are shaped between two adjacent elements, which makes FEM a continuous model. In DDA, all blocks are isolated and bounded by preexisting discontinuities. When blocks are in contact, Coulomb's law applies to the contact surface, and the simultaneous equilibrium equations are selected and solved for each loading or time increment. The blocks in DDA can be either convex or concave (or even multiconnected polygons with holes), whereas FEM usually only encompasses standard-shaped elements.

The stability of whole mechanical systems in the real world comes mainly from inertia forces and friction forces. DDA follows these laws and places them within the realm of mechanical analysis, thus stabilizing the numerical computation. When forces of inertia are taken into account, time should be considered as a parameter. Therefore, DDA is truly a numerical dynamic model. Because the assumption of infinitesimal displacement theory needs to be fulfilled in linear-elastic mechanics, the choice of very small time intervals should be specified. When the total potential energy of all the stresses and external forces is minimized, the submatrices of the inertia force terms have the following properties: (1) They are two orders of magnitude higher than internal stress or stiffness submatrices; (2) the coefficient terms of such matrices are proportional to (1/time^2); and (3) they are concentrated at the diagonal positions in the global coefficient or stiffness matrix. Thus, large numbers are distributed in all diagonal terms in the global stiffness or coefficient matrix, and the assumption of infinitesimal displacement theory is fulfilled. Besides playing a dominant role in the global stiffness matrix, inertia forces also play an important role in resisting rigid body motion, which is indispensable in dealing with the motions of a discontinuous block system. When two blocks lose contact, they will depart from each other with high speed if inertia is not considered in the numerical analysis. In this case, the assumption of infinitesimal displacement theory will not be satisfied, and divergence will occur in numerical calculations.

DDA is unique due to the concept of "block system kinematics," which regulates the movements of all the blocks, or finds the locations of all contacts among the blocks. Because the infinitesimal displacement theory is adopted, the rigid body rotation and the deformations of each block can be approximated using the coordinate dependent linear functions described here. If the locations of all contact forces are found, the governing equations of the motions of the block system become simultaneous linear equations. Shi's (1988) block system kinematics uses the following constraints to obtain the contact locations: no tension and no penetration between blocks. The mathematical descriptions of both constraints are given by a set of inequalities. Although minimizing the total potential energy with inequality constraints is a difficult nonlinear problem, Shi was able to break through the numerical impasse. When the block system moves and deforms, the blocks are in contact only along the boundary, and the nonpenetration inequalities can be transformed into the equations when two blocks are in contact.

There are three different kinds of contacts between blocks in the two-dimensional case: angle to edge, angle to angle, and edge to edge (Fig. 1). The edge-to-edge case can be transformed to two angle-to-edge contacts. An angle-to-edge contact is only possible if the following conditions are satisfied: (1) The distance from the angle vertex to the edge is less than twice the maximum displacements of points of all blocks; and (2) there is no overlapping when the angle vertex translates to the edge without rotation. An angle-to-angle contact is only possible if the following conditions are satisfied: (1) The distance between the vertices of two angles is less than twice the maximum displacements of points of all blocks; and (2) there is no overlapping when two angles are translated without rotation until the vertices coincide. Therefore, the contract problem is reduced to point-line crossing inequalities.

When interpenetration occurs at a given position, a "lock" is applied. A pair of stiff springs are added from the point that lies along the directions normal and parallel to the reference line. Coulomb's friction law will determine whether to keep or remove the other spring which is parallel to the reference line. By adding very stiff springs, or penalties, to lock the movements in one or two directions for the position of interpenetration, the penetration constraint equations can be imposed on the global governing equations. The physical meaning of applying stiff springs is to push back the invading angle along the shortest path. Accordingly, if a tensile contact force occurs between two blocks, the blocks will separate from each other after removal of the locks; hence, the nontension constraining inequalities can be reduced to the process of adding or removing the locks. Therefore, the so-called open-close iterations repeatedly select the locked positions, or unlock the constraining ones, until the condition of no penetration and no tension are satisfied for all contacts among the blocks. All the penalty submatrices are then imposed into the global stiffness matrix.

In DDA, Coulomb's law is used to calculate the shearing forces at the contact and is the criterion to evaluate the sliding or locking between the blocks. When the displacement (d) of the point (P_1) normal to the reference line ($\overline{P_2P_3}$) is positive [Fig. 2(a)], the normal component of the contact force is tensile; therefore, no lock or stiff spring is applied and the contact is opened. If the displacement is negative [Fig. 2(b)], the normal contact force is compressive and the contact is closed. When the shear component of the contact force is large enough to cause sliding, a stiff spring normal to the reference line is applied to allow sliding to take place along the reference edge. In contrast, if the shear component of the contact force is less than that calculated from Coulomb's law, the contact spring will be fixed in both directions and no sliding is permitted. Friction forces between the interfaces of blocks are obtained from the result of open-close iterations of block kinematics in the block system. The energy corresponding to the motion of the sliding forces represents the only energy consumption considered in the original DDA formulation. Energy can also be dissipated when nonlinear material behavior is included.

Although DDA considers both statics and dynamics, the only difference between these two cases is that the static computation assumes that the velocity is zero at the beginning of each time step, while the dynamic computation inherits the

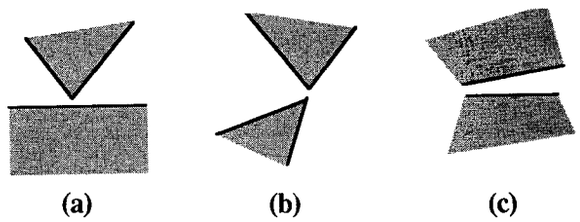

FIG. 1. Different Kinds of Contacts: (a) Angle to Edge; (b) Angle to Angle; (c) Edge to Edge

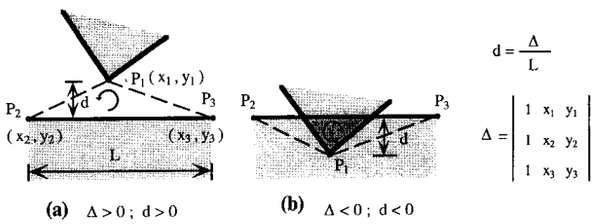

FIG. 2. Contact Judgment by Orientation of Vertices of Triangle $P_1P_2P_3$

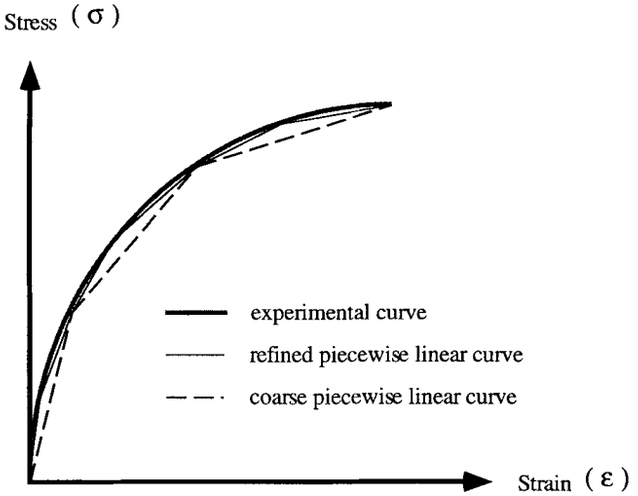

FIG. 3. Arc-Length Method

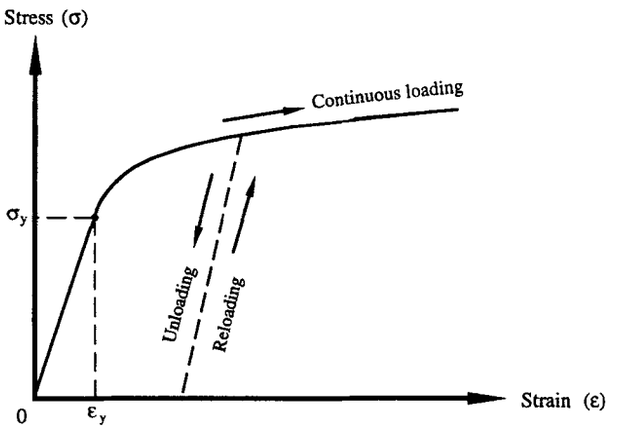

FIG. 4. Nonlinear Inelastic Stress-Strain Modeling

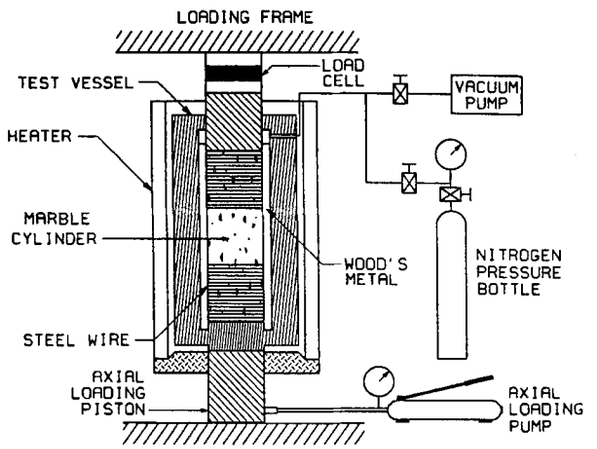

FIG. 5. Experimental Setup

velocity from the previous step. The process of step-by-step calculations assumes each step begins with the deformed block shapes and positions of the previous step. The equilibrium equations are solved for updated geometry and updated initial conditions, i.e., velocities, stresses, etc. Large displacements and deformations of the blocks are obtained by the accumulation of small displacements and deformations in each time step. This is the reason why DDA is characterized as the step-by-step linear kinematics, and is in the true spirit of Calculus developed by Newton. As the blocks move or deform, the updating block shapes and positions will produce different block contacts and the corresponding interactive forces. Thus,

TABLE 1. List of Basic Stereological Symbols and Their Definition

Symbol (1)	Dimensions (2)	Definition (3)
P	μm^{-1}	Number of point elements, or test points
P_L		Number of intersections of cracks in a section with a superimposed system of equally spaced test array of straight parallel lines per unit of line length
$P_L(\theta)$	μm^{-1}	Number of crack intersections in a section with a system of equally spaced test array of straight parallel lines positioned in such a way that it successively encloses an angle θ, $\theta = \pi/2$, and $\theta = 0$, respectively, with the axis of symmetry
L	μm	Length of lineal elements or test-line length
L_A	$\mu m/\mu m^2$	Total crack length in a section per unit of area
S	μm^2	Surface or interface area (not necessarily planar)
S_V	$\mu m^2/\mu m^3$	Total crack surface area per unit of volume (S/V_T)

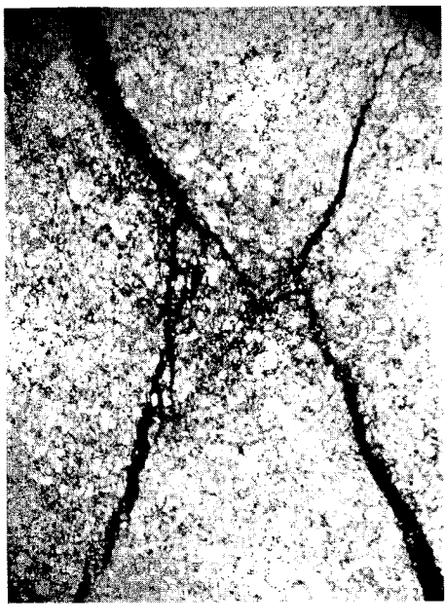

FIG. 6. Vertical Cross Section of Marble Specimen

the whole block system changes, affecting modes of failure more profoundly than those in continuum mechanics.

In DDA, the complete first-order polynomial function is chosen as the displacement function of a block. Shi (1988) transformed these six variables into another six variables with physical meanings

$$(u_0 \quad v_0 \quad r_0 \quad \varepsilon_x \quad \varepsilon_y \quad \gamma_{xy})$$

where (u_0, v_0) = rigid body translation of a specific point, (x_0, y_0), within the block; r_0 = rotation angle of the block with the rotation center at (x_0, y_0); and ε_x, ε_y, γ_{xy} = normal and shear strains of this block. Because an infinitesimal displacement theory is adopted, the displacement function of a given block can be represented by the coordinate dependent linear function written as

$$\begin{pmatrix} u \\ v \end{pmatrix} = \begin{bmatrix} 1 & 0 & -(y-y_0) & (x-x_0) & 0 & (y-y_0)/2 \\ 0 & 1 & (x-x_0) & 0 & (y-y_0) & (x-x_0)/2 \end{bmatrix} \begin{pmatrix} u_0 \\ v_0 \\ r_0 \\ \varepsilon_x \\ \varepsilon_y \\ \gamma_{xy} \end{pmatrix} \quad (1)$$

Combination of DDA with Finite-Element Mesh

The main purpose of placing a finite-element mesh in each block is to improve its deformation ability. Although in DDA

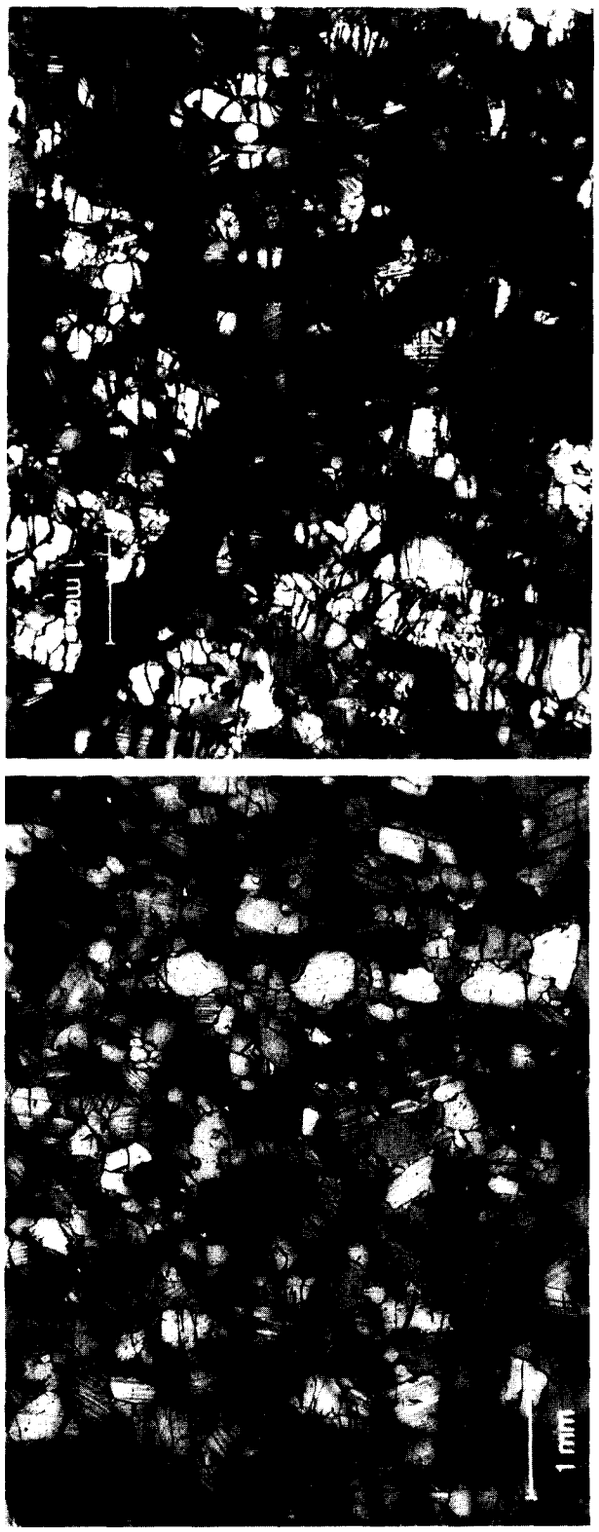

FIG. 7. Cracking in: (a) Center; (b) Extremity of Specimen

the geometry of the block can be convex or concave (even with holes in it), the stress and strain in each block is constant, not a realistic assumption for a big block. Thus, the addition of a finite-element discretization in each block eliminates this shortcoming. Not only will the movements of the block system be depicted by DDA, but also the stress distributions within the blocks will be obtained.

If the finite-element mesh of constant strain elements is chosen, the complete first-order polynomial displacement function is used to describe the triangular element's behavior. There are six nodal displacements to be chosen as unknown variables. These are

$$(u_1 \quad v_1 \quad u_2 \quad v_2 \quad u_3 \quad v_3)$$

The functions of the geometry of the blocks is used as the contact boundaries for the purpose of block kinematics in the block system. Thus, the shape of the block need not be triangular. By adding a finite-element mesh in each block, more nodes are distributed along the contact boundaries of the block, and the contact detection from block system kinematics become more complicated in a discontinuous system.

Consider a three-node element where the boundaries are drawn along the nodes in certain directions, forming a three-edge block with the same size as the element. This configuration is called a three-node "element block"—a block with nodal displacements as unknowns. If a three-node element is extended to an n-node element mesh, an element-mesh block with n nodes is obtained. In general, a block can be as small as an element or as large as an element mesh. Different meshes can also be put into different blocks if conditions permit.

The computer program dictates that the meshes of the elements and the boundaries of the blocks be input separately. Then, element meshes and blocks are merged with the same nodal numbers between the elements, but with different nodal numbers between the boundaries of the blocks. The basic element in this numerical model is a triangular element. For the convenience of putting the mesh in each block, four-node element meshes are first generated in the mesh program. Then, a condensed five-node element—a quadrilateral element with four nodes on its vertices and one additional node inside it that forms four triangular elements—is used for forward model computations.

Based on the idea of element-mesh blocks, the mesh in FEM is just one block in DDA. By adding the finite-element mesh into each block, it is possible to take advantage of the continuous properties in FEM and discontinuous characteristics of DDA, thereby simulating engineering problems more accu-

FIG. 8. Backscattered Image of Center of Specimen (White Areas Are Cracks Filled by Wood's Metal)

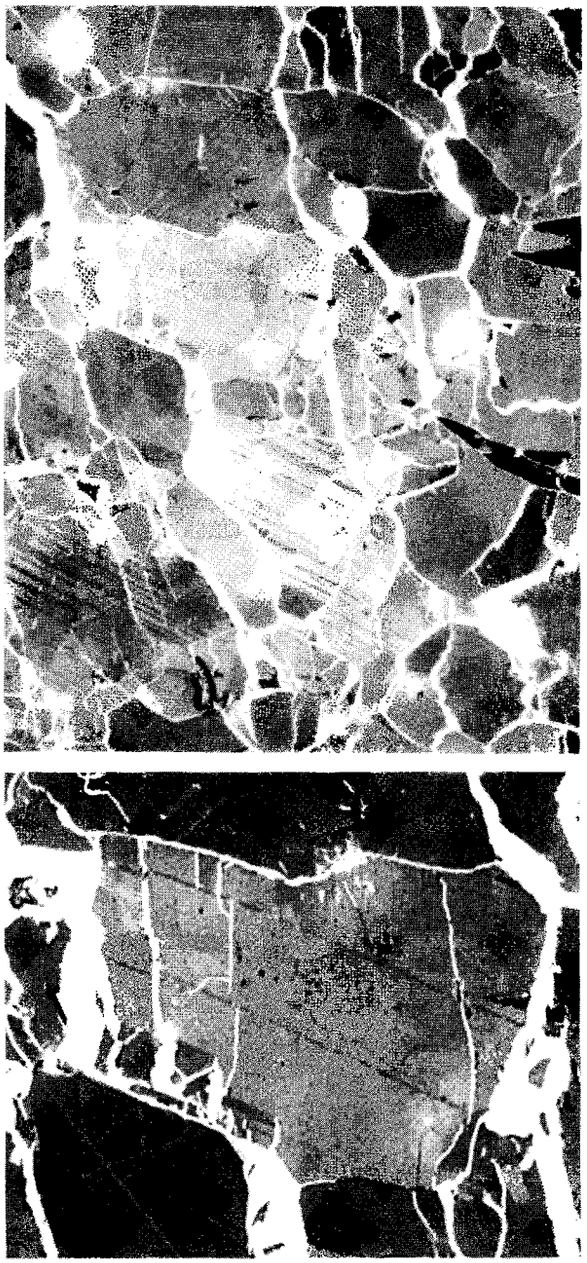

FIG. 9. (a) Backscattered Image of Extensile Cracks (White) Generated by Point Loads; (b) Detail from Fig. 9(a) Showing Extensile Cracks in Marble Crystal

rately. Details of these derivations can be found in Shyu (1993).

Simultaneous Equilibrium Equations

The simultaneous equilibrium equations derived by minimizing the total potential energy, Π, have the following form:

$$\begin{pmatrix} [K_{11}] & [K_{12}] & [K_{13}] & \cdots & [K_{1n}] \\ [K_{21}] & [K_{22}] & [K_{23}] & \cdots & [K_{2n}] \\ [K_{31}] & [K_{32}] & [K_{33}] & \cdots & [K_{3n}] \\ \vdots & \vdots & \vdots & \ddots & \vdots \\ [K_{n1}] & [K_{n2}] & [K_{n3}] & \cdots & [K_{nn}] \end{pmatrix} \begin{pmatrix} \{D_1\} \\ \{D_2\} \\ \{D_3\} \\ \vdots \\ \{D_n\} \end{pmatrix} = \begin{pmatrix} \{F_1\} \\ \{F_2\} \\ \{F_3\} \\ \vdots \\ \{F_n\} \end{pmatrix} \quad (2)$$

As in the FEM, the nodal displacements are chosen as unknown variables and each has two degree of freedom for the two-dimensional case. For the given ith node, $[K_{ij}]$ is a 2×2 submatrix representing the stiffness of displacement at the ith node with respect to the load acting on the jth node. $\{D_i\}$ and $\{F_i\}$ are 2×1 submatrices for the corresponding unknown nodal displacement and nodal loading matrices.

Inertia Matrix

Because the inertia force plays a key role in rigid body motion, it is crucial to include it in dealing with the motions of a discontinuous block system. Assuming the acceleration in each time step is constant, the 2×2 nodal stiffness matrices and 2×1 force matrices of element i can be described as

$$[\mathbf{K}_{i(r)i(s)}] = \frac{2M}{\Delta^2}\left[\int\int_A [T_{i(r)}]^T[T_{i(s)}]\,dx\,dy\right] \quad r, s = 1, 2, 3 \quad (3)$$

$$[\mathbf{F}_{i(r)}] = \frac{2M}{\Delta}\left[\int\int_A [T_{i(r)}]^T[T_{i(s)}]\,dx\,dy\right] \cdot \{\mathbf{V}_{i(s)}(0)\} \quad \begin{cases} r = 1, 2, 3 \\ s = \text{tensor sum} \end{cases} \quad (4)$$

where

$$\{\mathbf{V}_{i(s)}(0)\} = \frac{\partial}{\partial t}\begin{pmatrix} u_{i(s)}(0) \\ v_{i(s)}(0) \end{pmatrix}$$

M = mass per unit area; and Δ = time interval of current time step. The analytical solutions (3) and (4) can be obtained (Chang 1994).

Normal Contact Matrix

When two bodies are detected to be in contact, the requirement of no penetration must be satisfied according to DDA's block kinematics. The contact problem reduces to the relationship of the angle-to-edge (point-to-line) case. When interpenetration pushes the point through the reference line, the distance between them should be zero after the installation of spring with stiffness p at the contact position. The nodal stiffness and force matrices of element i and j are described as

$$[\mathbf{K}_{i(r)i(s)}] = p\{H_r\}\{H_s\}^T \quad r, s = 1, 2, 3 \quad (5a)$$

$$[\mathbf{K}_{i(r)j(s)}] = p\{H_r\}\{G_s\}^T \quad r, s = 1, 2, 3 \quad (5b)$$

$$[\mathbf{K}_{j(r)i(s)}] = p\{G_r\}\{H_s\}^T \quad r, s = 1, 2, 3 \quad (5c)$$

$$[\mathbf{K}_{j(r)j(s)}] = p\{G_r\}\{G_s\}^T \quad r, s = 1, 2, 3 \quad (5d)$$

$$\{\mathbf{F}_{i(r)}\} = -p\left(\frac{S_0}{L}\right)\{H_r\} \quad r, s = 1, 2, 3 \quad (6a)$$

$$\{\mathbf{F}_{j(r)}\} = -p\left(\frac{S_0}{L}\right)\{G_r\} \quad r, s = 1, 2, 3 \quad (6b)$$

where

$$\text{for element } i \begin{cases} i(1) = i_1 \\ i(2) = i_2 \\ i(3) = i_3 \end{cases} \quad \text{for element } j \begin{cases} j(1) = j_1 \\ j(2) = j_2 \\ j(3) = j_3 \end{cases}$$

The detailed derivation of internal stress, external loading, displacement constraint, and contact matrices are described in Shyu (1993).

Nonlinear Material Behavior

In structural mechanics literature, a problem is called nonlinear if the stiffness matrix or the load vector depends on the displacements. This nonlinearity can be classified as (1) material nonlinearity, which is associated with changes in material properties, as in plasticity; and (2) geometric nonlinearity, which is associated with changes in configuration, as in large displacements or deformations of the structures. Geometric nonlinearity is modeled in DDA using a discrete time system.

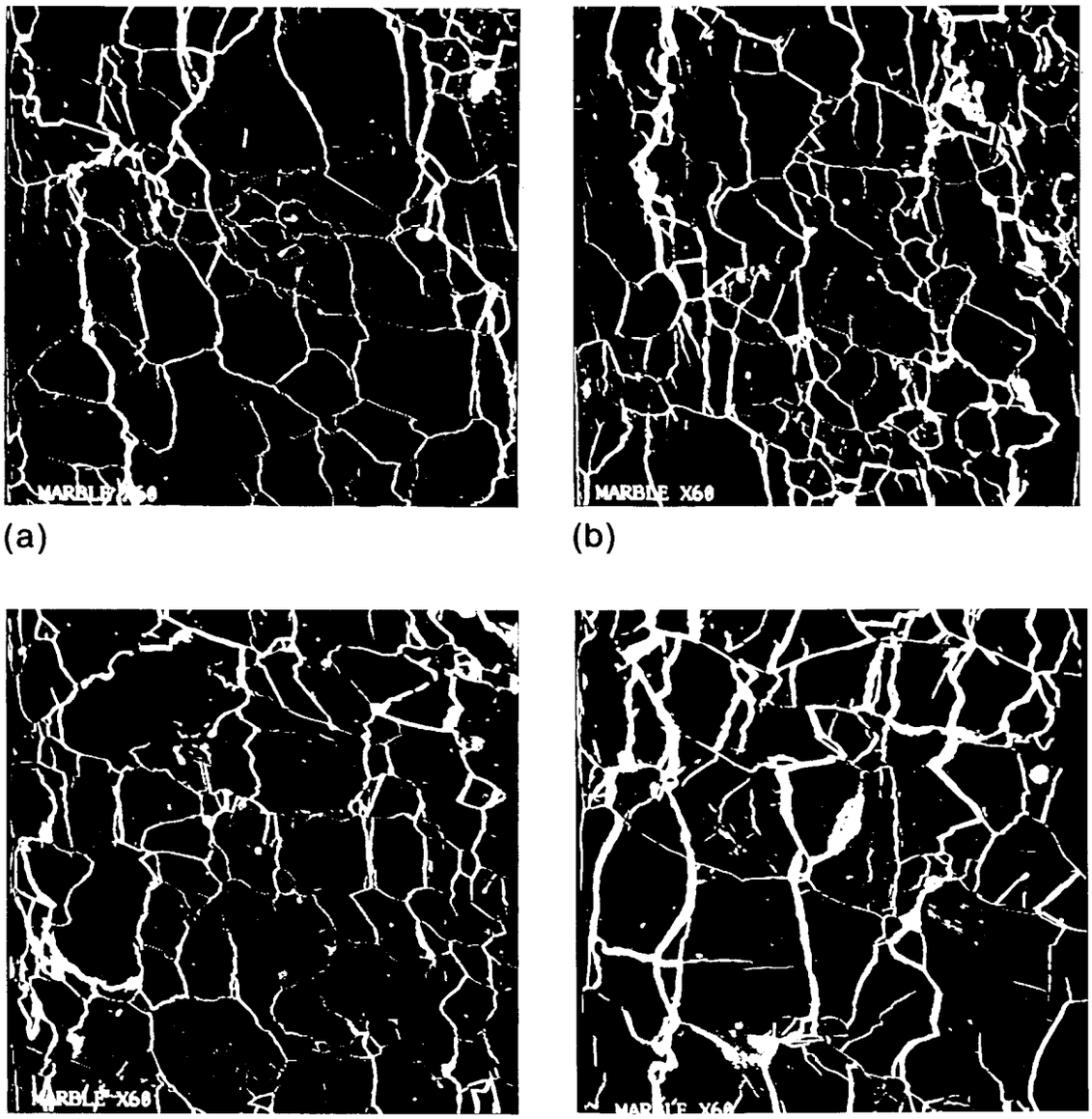

FIG. 10. Typical Backscattered Images Used to Establish Stereological Parameters

FIG. 11. Secondary Electron Image of Etched Sample Showing Grain Boundary Microcracks

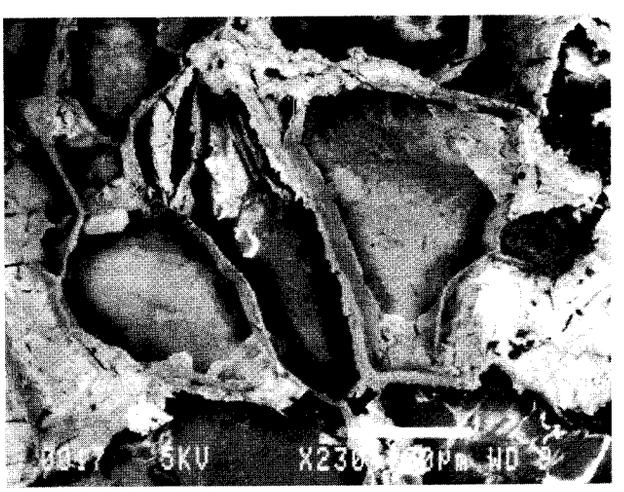

FIG. 12. Secondary Electron Image of Etched Sample Showing Grain Boundary and Extensile Microcracks

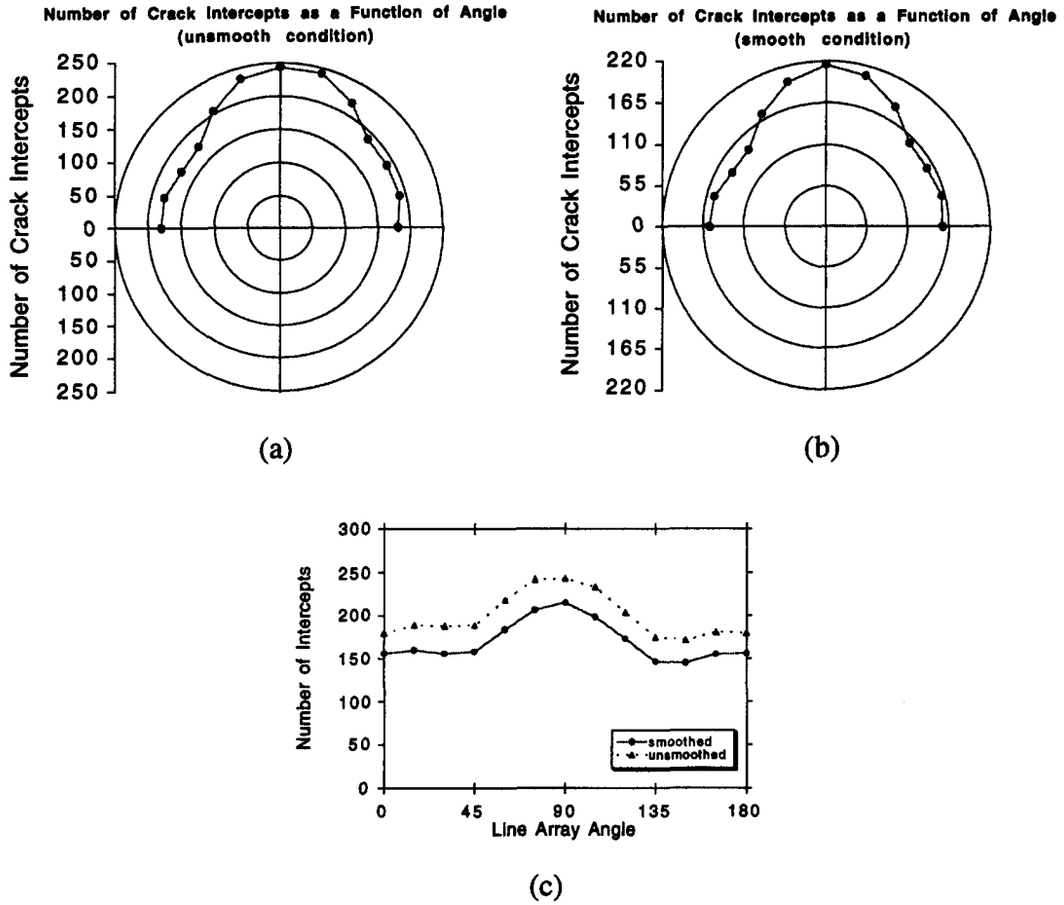

FIG. 13. Number of Crack Intercepts in Function of Line Array Angles

The present work develops material nonlinearity formulation and implementation for input into DDA.

DDA uses a step-by-step approach. Each step starts with the deformed shape and positions from the previous step; the stresses from the previous step are considered as the initial stresses at the current step. After adopting the updated geometry, contact positions, velocities, and stresses from the previous time step, the computation for the current step is independent from the data of the previous step. All the deformability constants, loading, initial stresses, and boundary conditions can be changed at the current step. Because the time interval of each time step is very small, the displacement, deformations, and changes of stresses are very small, so that the tangent modulus of the stress-strain relationship at the current step is very close to the secant modulus of the stress-strain curve. Thus, the arc-length method (Fig. 3) can be used to calculate the piecewise linear modulus based on the updated values of stresses and strains for the nonlinear constitutive behavior of materials. The preclusion of the volumetric strain is neglected in plasticity for the present model.

The use of line segments to depict the nonlinear behavior of the material is another way to show that the linear step-by-step approach can solve both material and geometric nonlinearity problems. Trying to solve nonlinear material problems using only one step may violate the infinitesimal displacement theory. When finite-element meshes and blocks are combined together to obtain the stress distributions, or to improve the deformation ability of the block, the use of a piecewise linear stress-strain curve to solve material nonlinearity step by step allows solutions of complex engineering problems.

The present work develops equations for nonlinear isotropic materials using principal strain as the criterion for the change of Young's modulus E and Poisson's ratio, ν. The more the line segments chosen follow the stress-strain curve, the better the approximation of nonlinear inelastic material behavior for each time step. Without the incorporation of fracture criterion, the element meshed block of the system always remains as an intact material in the present model. The material is assumed to be strain hardening after yielding, because the strain-softening behavior observed in the experimental stress-strain curve reflects the global specimen instead of the individual blocks. The true stress-strain curve is used in the model, plus the Bauschinger effect is considered in cyclic loading. The unloading and reloading paths after yielding are assumed to be the same in the stress-strain curve, as shown in Fig. 4.

EXPERIMENTAL METHODS

An apparatus similar to the one used by Nemati (1994) was used for this experiment. To preserve the microstructure in marble specimens under load, the voids and fractures were filled with Wood's metal during loading, and the alloy was solidified in place before unloading. The composition of the Wood's metal was: 42.5% Bi, 37.7% Pb, 11.3% Sn, and 8.5% Cd, and it had a melting point of approximately 80°C. A cylindrical core was cut and the ends were ground parallel to one another at the required length. After this stage, the specimen was ready for uniaxial compression test assembly. The vessel containing the molten metal and the specimen was assembled with loading and measuring apparatus. The linear variable displacement transducers (LVDTs) for the axial displacement measurements were attached to a steel end piece, and the LVDT for the radial displacement measurement was at-

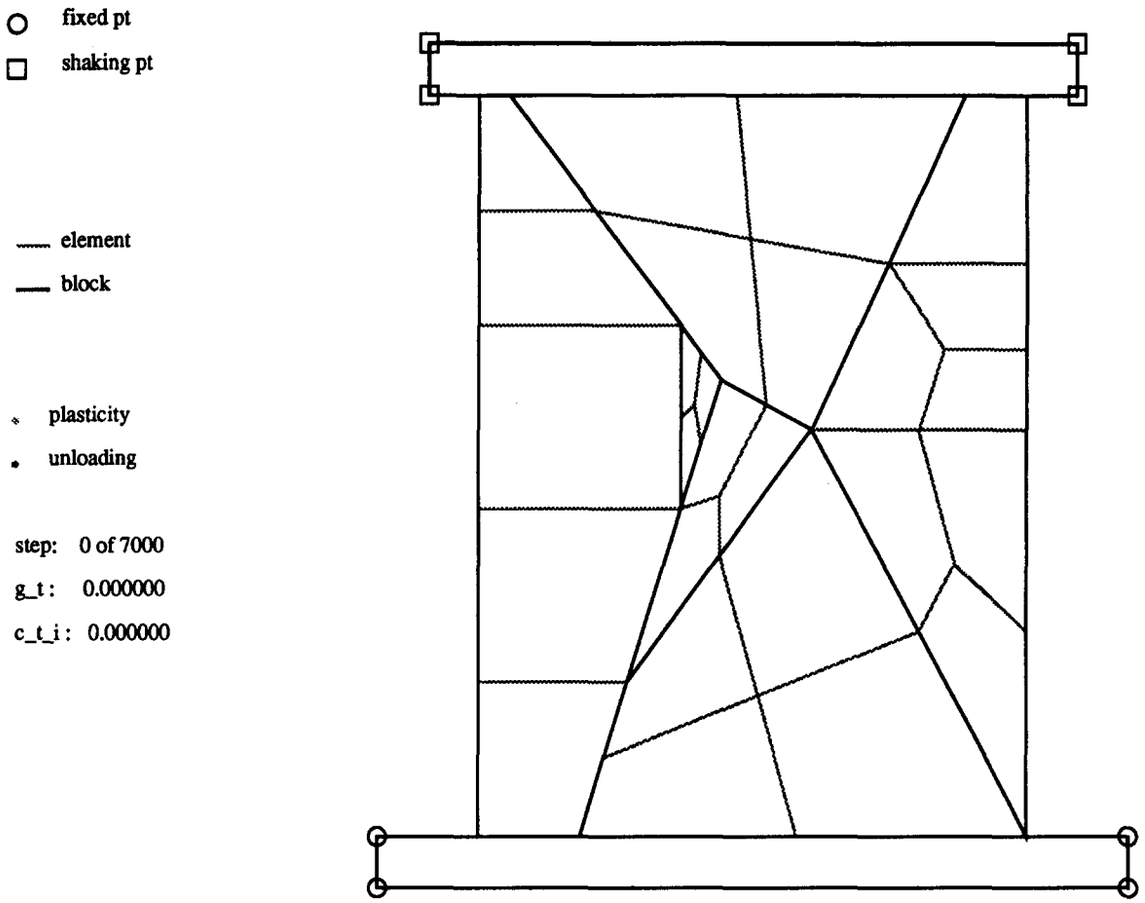

FIG. 14. Original Configuration of Element Block System

tached to a split steel ring. Fig. 5 shows a schematic setup for the testing.

The internal temperature was established and maintained at 96°C (205°F) during the test, and a vacuum was applied to the vessel and kept constant for at least 30 min. The vacuum removed any air that had become trapped in the marble cylinder when it was assembled inside the vessel. An axial stress of 90% of the ultimate strength was applied to the marble cylinder, at which point the vacuum was removed. Finally, the induced microcracks were saturated with the molten metal with a pore pressure of 10.3 MPa (1,500 psi). The pressure was kept constant throughout the test and did not alter the effective stresses on the marble cylinder. With a surface tension of 400 N/m, the alloy could penetrate into flat cracks with apertures as fine as 0.08 μm. The axial strain of interest was kept constant for 10 min to allow the liquid to penetrate into pores and fractures fully before the vessel was rapidly cooled down to room temperature. The marble test specimen was then sectioned along its axis and across its diameter, and then ground and polished for microscopic examination and photography.

Stereology of Marble Samples

All matter can be described in terms of zero, one, two, and three dimensions. Stereology deals with the interpretation of three-dimensional structures by means of their two-dimensional sections. Stereology is the opposite of photogrammetry, which utilizes three-dimensional images in order to construct flat maps. Techniques conventionally used for studying the three-dimensional structure of materials, particularly in other material sciences, are often stereological ones.

If a sectioning plane cuts a three-dimensional aggregate of space-filling polyhedrons, a two-dimensional structure that consists of area-filling polygons can be observed. The task then is to relate the observations made on a section to the true three-dimensional microstructure. Stereology attempts to numerically characterize the geometrical aspects of those features of the microstructure of interest; for example, the microcracks in concrete represented by Wood's metal. In its broadest context, stereology includes not only the quantitative study and characterization of any spatial structure, but also its qualitative interpretation.

There are various approaches to stereological problems. The statistico-geometrical approach depends on measuring and classifying a large number of two-dimensional images; this is the method used in this study. It is applicable when objects are randomly distributed in space. In such cases, a single section, if extensive enough to contain a statistically significant number of features, may suffice to obtain valid results. This study considers the numerical or quantitative characterization of points, lines, surfaces, and volumes. Fundamental expressions were determined that relate measurements on two-dimensional sections to the three-dimensional structure. Table 1 presents some of the basic symbols commonly used in the measurements employing quantitative stereology.

In this research, the stereological parameters of P_L, L_A, and S_V will be used to perform the stereological analysis. The relationships between L_A and S_V with P_L is presented as follows (Underwood 1968):

Surface-to-volume ratio, S_V

$$S_V = 2P_L \ \mu m^2/\mu m^3 \tag{7}$$

Length of line per unit area, L_A

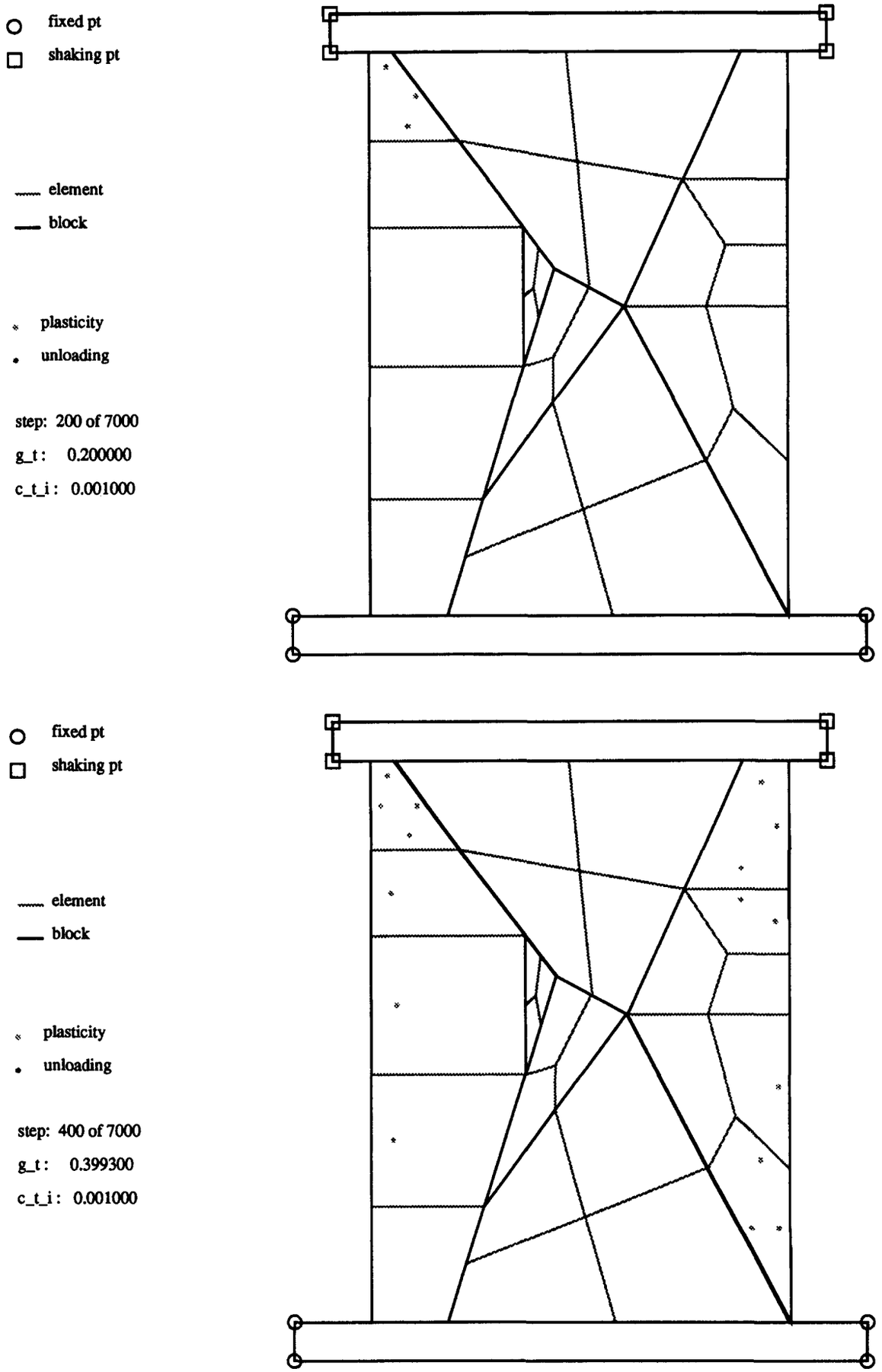

FIG. 15. Propagation of Plastic Regions; Failure Mode and Progressive Dilation of Marble Sample Can Be Observed

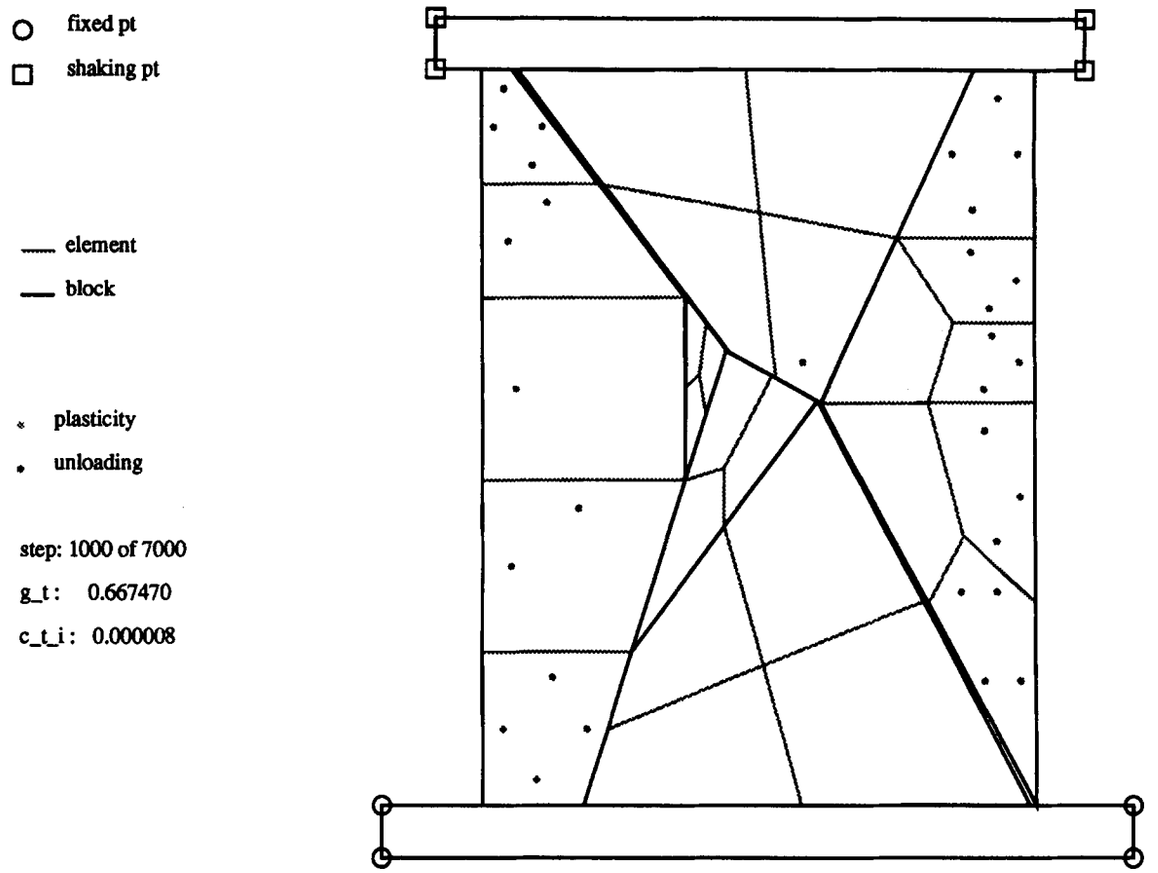

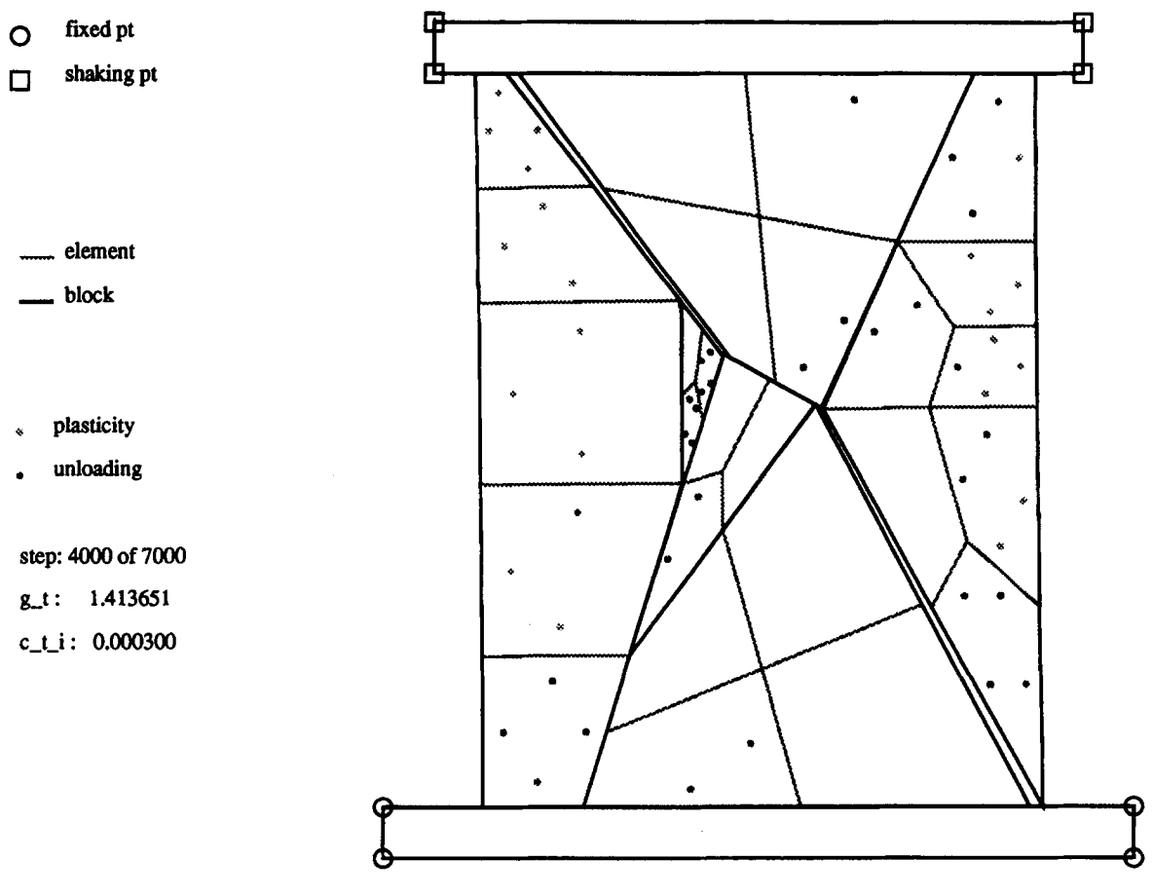

FIG. 15. (*Continued*)

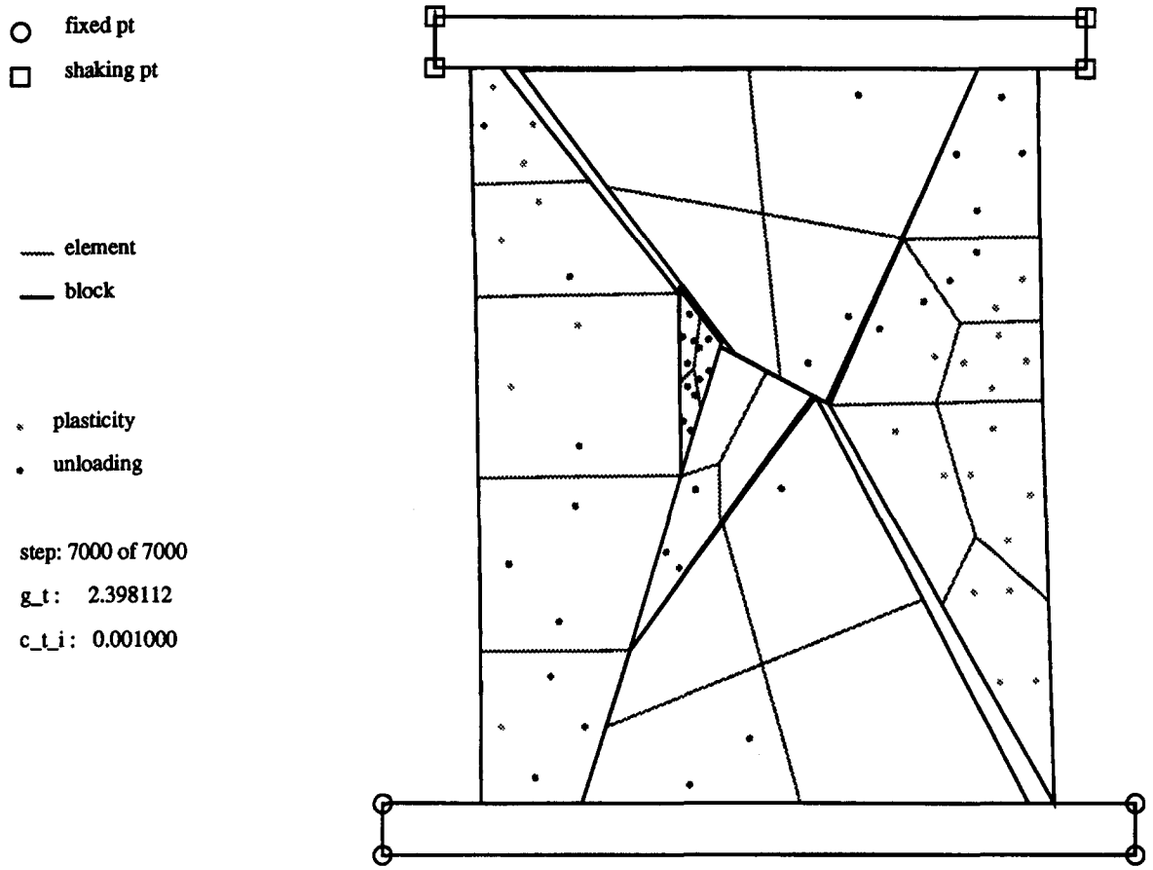

FIG. 15. (*Continued*)

$$L_A = \left(\frac{\pi}{2}\right) P_L \ \mu m/\mu m^2 \tag{8}$$

or

$$\frac{\pi}{2} P_L = L_A = \frac{\pi}{4} S_V \tag{9}$$

Applying the method of random secants on a plane to an image of a crack pattern, (9) presents simple algebraic relationships to calculate the total crack length per unit area or the specific surface area (of the cracks) per unit volume. The dependence of the number of intersections per unit length with the angle of the test array can be used to characterize the degree and types of orientation of a system of lines in a plane. Saltikov (1945) proposes a polar plot of P_L with respect to the orientation axis (axes), and calls the resulting curve the rose of the number of intersections, or simply the rose.

The rose for an oriented system of lines can be easily obtained experimentally. We apply a test array to the system of lines at (equal) angular increments with respect to the orientation axis, and determine P_L separately at each angle. Then we draw radius vectors on a polar graph paper, plotting P_L versus θ. We connect the ends of the radius vectors by a smooth curve, giving the rose. In case of isometry, the rose will be a circle with its center at the origin of the polar figure. If a preference direction should occur in a crack pattern, the shape of the rose will change.

The stress-induced microcrack system in marble is considered to be partially oriented, as opposed to a completely oriented (idealized) system. Test arrays of equal angular increments were applied to each binary image, and the number of intersections was determined separately at each angle θ. Then the number of intersections was plotted versus θ, creating the "compass rose" pattern diagram.

The rose diagram characterizes the degree of orientation of the cracks, making it easier to interpret the data. The rose diagrams were plotted to cover only the range of 0°–165° (cracks at 0° and 180° have equal lengths) since the range from 180° to 360° is redundant.

Many researchers have successfully applied the concept of stereology to study micromechanical aspects of engineering materials. With the advent of modern image analysis systems, it is now possible to perform stereological analysis on a great number of images accurately and expeditiously, whereas in the past this was not achievable by manual methods.

EXPERIMENTAL RESULTS

Fig. 6 shows the vertical cross section of a marble specimen that has been loaded up to failure. The dark zones indicate where the metal has penetrated the crack induced by the mechanical load. There is strain localization at the center of the specimen and development of four major lines of shear failure starting at the edges of the specimen. This image will be used as a starting point for the modeling developed in the following section. Fig. 7(a) shows an optical image of the center of the specimen where intense cracking localization developed. Due to the three-dimensional confinement caused by end effects, the amount of damage is not as intense at the extremities of the sample, as indicated by Fig. 7(b).

A large number of intragranular cracks were observed, as shown in Figs. 8 and 9. Similar cracks were noted by Zheng (1989) in his comprehensive work on limestone microcracking, by Baztle et al. (1980), and Dey and Wang (1981). Many of the intragranular cracks were generated as a result of point

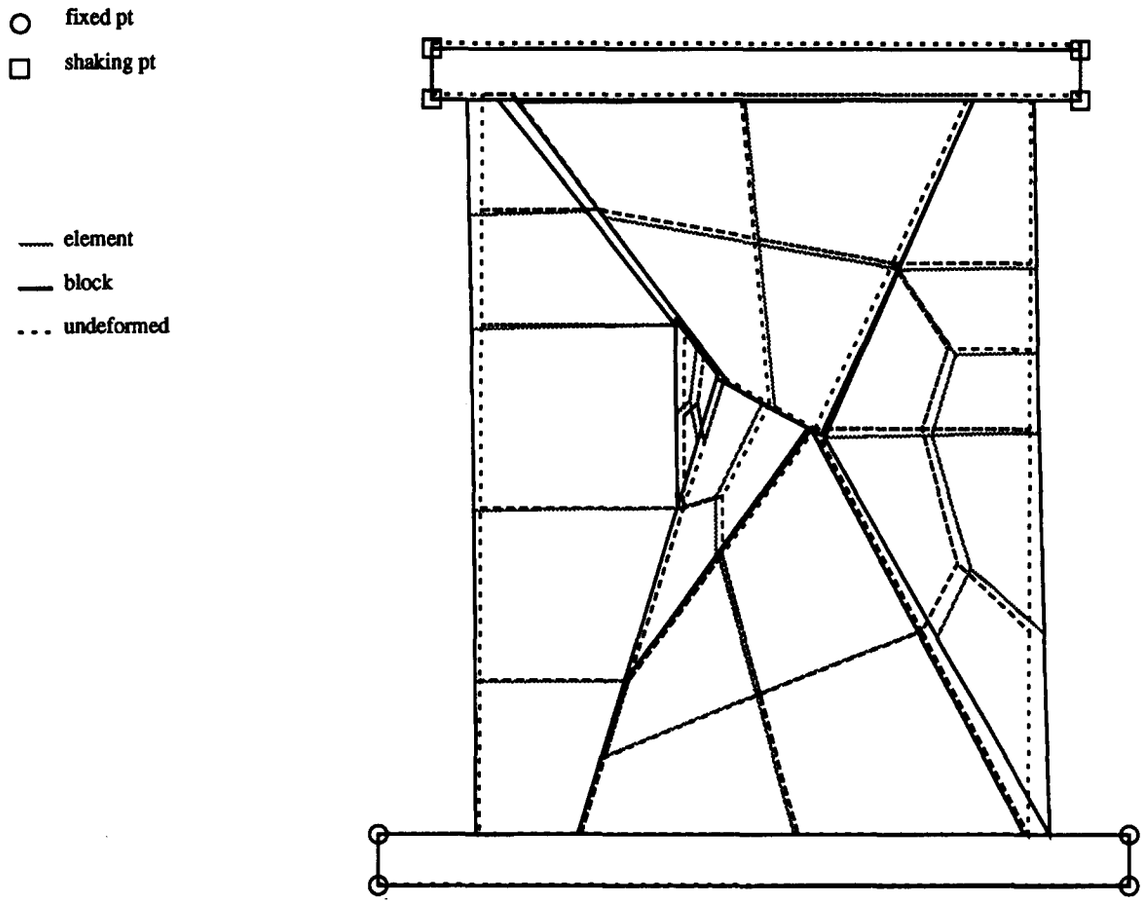

FIG. 16. Deformed and Undeformed Shapes of Specimen

loading. As observed by Zheng, grain boundary microcracks can often develop into intragranular cracks, or remain intergranular cracks, particularly if the grain boundary is parallel to the maximum compression direction. When grains are loaded across their diameter, microcracks develop inside the grains caused by the tensile stresses generated in a condition similar to a Brazilian splitting test. Fig. 9(a) shows such microcracks aligned along the loading points.

The quantitative analysis was performed in polished samples of marble, using backscattered electron imaging. Fig. 10 shows a typical image using such a technique. A few samples were exposed to mild acid so the marble would leach away, leaving the three-dimensional framework formed by the cracks filled with Wood's metal. Under a secondary electron microscope these samples indicate the complexity of the system of cracks induced by the stress. Figs. 11 and 12 show the three-dimensional crack network. These images, even though useful for visualization, are not quantitative, so most of the research effort concentrated on the analysis of backscattered images.

Fifty-six backscattered images went through computer manipulations to establish the statistical parameters. For each parameter, an average, standard deviation, standard error, and ratio of standard error over average were calculated. Standard error was calculated as follows:

$$\text{standard error} = \frac{\sigma}{\sqrt{\text{Number of Im}}} \tag{10}$$

The ratio of standard error over the average of 5% is considered to be a good result. The microcrack density distribution represents the number of microcracks per unit of observation area. Pore spaces are not counted as microcracks. Fig. 13 shows the number of crack intercepts as a function of line array angles. Together they represent the open version of the rose diagram. There is a strong indication that the microcracks are subparallel to the direction of the maximum compression. From a fracture mechanics point of view, the stress intensity factors form the opening microcracks in the direction of the maximum compressive stress.

COMPRESSIVE POSTFAILURE ANALYSES OF MARBLE SPECIMEN

This simulation analyzes the compressive postfailure behavior of a marble specimen with preexisting cracks. The main cracks observed experimentally (see Fig. 6) were used as the original configuration of the element block system (Fig. 14). The marble specimen is 3.65 cm long, 2.54 cm wide, and the mesh contains 28 elements and eight blocks. The upper and lower rectangular blocks are simulated as the loading and base frames. The simulation is done under displacement control. The loading rate is 0.013 cm/s. The effect of lateral confinement on the specimen is also investigated. The following parameters were used:

Case: plane strain dynamics
Stiffness of the contact spring (penalty): 1.46×10^8 kN/m
Time interval: 0.001 s
Unit mass: 2,713 kg/m^3
Gravity: 9.81 m/s^2
Friction angle: 35°
Initial stress (σ_x, σ_y, τ_{xy}): (0, 0, 0) MPa
Yielding strain (ε_t, ε_c) for the marble specimen: (0.001, −0.001)
Range of ε_1 for (E_1, ν_1) of the marble specimen in compression: E is in MPa

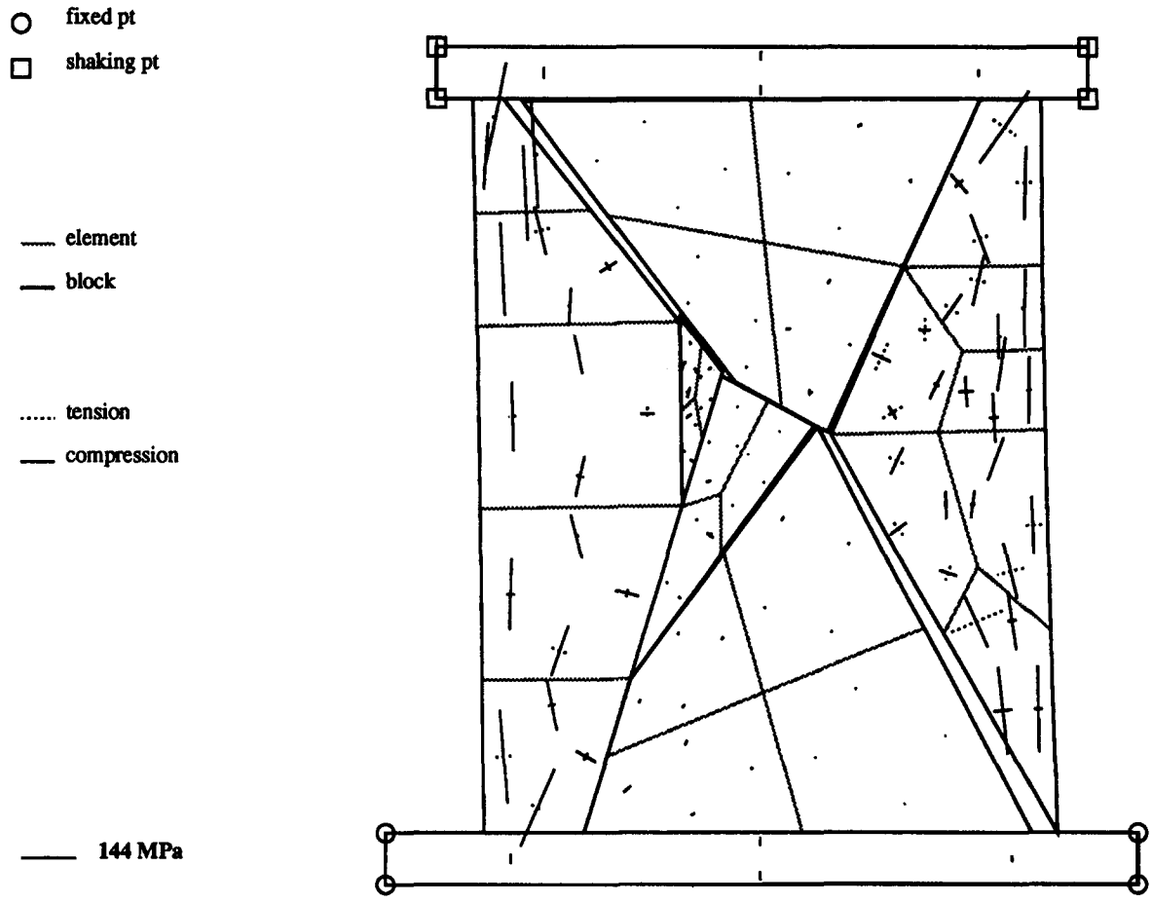

FIG. 17. Principal Stresses and Directions after Final Step, with Dashed Lines Represent Tension and Solid Lines Compression

For loading
Range 1: $-0.001 < \varepsilon \leq 0.000$, $(E_1, \nu_1) = (5.14 \times 10^4, 0.17)$
Range 2: $-0.900 < \varepsilon \leq -0.001$, $(E_1, \nu_1) = (2.07 \times 10^4, 0.17)$
For unloading
Range (1): $-0.900 < \varepsilon \leq 0.000$, $(E_1, \nu_1) = (5.14 \times 10^4, 0.17)$
E_2, ν_2 of the loading and base blocks (elastic material): 2.07×10^5 MPa, 0.3

Seven thousand time steps (≈2.398 s) were used in the computation. Fig. 15 shows the results after steps 200, 400, 1,000, 4,000, and 7,000. Figs. 15(a–e) indicate the propagation of plastic regions. Round tint marks represent the area where the material reached the inelastic range and stayed in the continuous loading track, while the round dark marks indicate the area that also was reached in plastic range, but lay in unloading track. The simulation was able to capture the failure mode and the progressive dilation of the marble sample, as observed experimentally in Fig. 6. Fig. 16 shows the deformed and undeformed shapes of the sample, and Fig. 17 presents the principal stresses and directions after the final step, with dashed lines representing tension and solid lines representing compression.

CONCLUSIONS

The Wood's metal technique allowed the study of microcracks in marble under compressive loads. The advantage of such an alloy is that it can be injected into voids and stress-induced microcracks at the desired stress level, then solidified at any stage of the experiment to preserve, in three-dimensional form, the geometry of the microcracks induced at any given stage of the experiment. Microscopy study showed that most of the microcracks were extensible, and stereology analysis revealed that the microcracks have a tendency to grow subparallel to the direction of maximum compression.

By incorporating finite-element mesh and nonlinear material behavior into each block, an enhanced version of discontinuous deformation analysis can be applied to investigate the global stability of the discontinuous system, in addition to clarifying the stress distribution and plastic region propagation in the element block system of the marble specimen. This discontinuous approach provides another way to understand the postfailure effect and global stability of the structural system.

APPENDIX. REFERENCES

Batzle, M. L., Simmons, G., and Siegviel, R. W. (1980). "Microcrack closure in rock under stress: direct derivation." *J. Geophys. Res.*, 85, 70–72.
Chang, C.-T. (1994). "Nonlinear dynamic discontinuous deformation analysis with finite element meshed block system," PhD dissertation, Dept. of Civ. Engrg., Univ. of California at Berkeley, Calif.
Cohen, J., and Monteiro, P. J. M. (1991). "Durability and integrity of marble cladding: a state-of-the-art review." *J. Perf. Constr. Fac.*, ASCE, 5(2), 113.
Cundall, P. A. (1971). "A computer model for simulating progressive, large-scale movements in blocky rock systems." *Proc., Symp. of Int. Soc. of Rock Mech.*, Int. Soc. for Rock Mech., 11–18.
Cundall, P. A. (1988). "Formulation of a three-dimensional distinct element model—Part I. A scheme to detect and represent contacts in a system composed of many polyhedral blocks." *Int. J. Rock Mech. and Min. Sci.*, 25, 107–116.
Dey, T. N., and Wang, C. Y. (1981). "Some mechanism of crack growth and interaction in compressive rock failure." *Int. J. Rock. Mech. and Min. Sci.*, 18, 199–209.
Goodman, R. E., Taylor, R., and Brekke, T. L. (1968). "A model for the

mechanics of jointed rock." *J. Soil Mech. and Found. Div.*, ASCE, 94(3), 637–659.
Hart, R., Cundall, P. A., and Lemos, J. (1988). "Formulation of a three-dimensional distinct element model—Part II. Mechanical calculations for motion and interaction of a system composed of many polyhedral blocks." *Int. J. Rock Mech. and Min. Sci.*, 25, 117–125.
Hoek, E., and Bieniawshi, Z. T. (1965). "Brittle fracture propagation in rock under compression." *Int. J. Fracture Mech.*, 1, 137–155.
McClintock, F. A., and Walsh, J. B. (1962). "Friction on Griffith cracks in rocks under pressure." *Proc., 4th U.S. Mat. Congr. Appl. Mech.*, Am. Soc. of Mech. Engrs. (ASME), New York, N.Y., Vol. 2, 1615–1621.
Nemati, K. M. (1994). "Generation and interaction of compressive stress-induced microcracks in concrete," PhD dissertation, Dept. of Civ. Engrg., Univ. of California at Berkeley, Calif.
Nemat-Nasser, S. (1985). "Geometric probability approach to the characterization and analysis of microcracking in rocks." *Mech. of Mat.*, 4, 277–281.
Saltikov, S. A. (1945). *Stereometric metallography*, 2nd Ed., Metallurgizdat, Moscow, Russia.
Shi, G. H. (1988). "Discontinuous deformation analysis—a new numerical model for the statics and dynamics of block systems," PhD dissertation, Dept. of Civ. Engrg., Univ. of California at Berkeley, Calif.
Shyu, K. (1993). "Nodal based discontinuous deformation analysis," PhD dissertation, Dept. of Civ. Engrg., Univ. of California at Berkeley, Calif.
Underwood, E. E. (1968). *Quantitative stereology*. Addison-Wesley Publishing Co., Reading, Mass.
Walsh, J. B. (1965). "The effect of cracks on the uniaxial compression of rocks." *J. Geophys. Res.*, 70, 399–411.
Yadev, G. D., Dullien, F. A., Chatzis, I., and MacDonald, I. F. (1984). "Microscopic distribution of wetting and non-wetting phases in sandstone during immiscible displacements." *Proc., SPE Annu. Conf.*
Zheng, Z. (1989). "Compressive stress-induced microcracks in rocks and applications to seismic anisotropy and borehole stability," PhD dissertation, Dept. of Engrg.-Mat. Sci. and Mineral Engrg., Univ. of California at Berkeley, Calif.
Zienkiewicz, O. C., and Taylor, R. L. (1991). *The finite element method*, 4th Ed., Vol. 1-2, McGraw-Hill Book Publishing Co., Inc., London, England.